

Potential of the next generation VHE instruments to probe the EBL (I): the low- and mid-VHE

Martin Raue^{a,*}, Daniel Mazin^b

^a*Institut für Experimentalphysik, Universität Hamburg, Hamburg, Germany*

^b*Institut de Física d'Altes Energies (IFAE), Edifici Cn. Universitat Autònoma de Barcelona, 08193 Bellaterra (Barcelona), Spain*

Abstract

The diffuse meta-galactic radiation field at ultraviolet to infrared wavelengths - commonly labeled extragalactic background light (EBL) - contains the integrated emission history of the universe. Difficult to access via direct observations, indirect constraints on its density can be derived through observations of very-high energy (VHE; $E > 100$ GeV) γ -rays from distant sources: the VHE photons are attenuated via pair-production with the low energy photons from the EBL, leaving a distinct imprint in the VHE spectra measured on earth. Discoveries made with current generation VHE observatories like H.E.S.S. and MAGIC enabled strong constraints on the density of the EBL, especially in the near-infrared. In this article the prospect of future VHE observatories to derive new constraints on the EBL density are discussed. To this end, results from current generation instruments will be extrapolated to the future experiment's sensitivity and investigated for their power to enable new methods and improved constraints on the EBL density.

Keywords: very-high energy gamma-rays, extragalactic background light, future instruments

PACS: 95.85.Pw, 98.70.Vc

*Corresponding author.

Email addresses: martin.raue@desy.de (Martin Raue), mazin@ifae.es (Daniel Mazin)

1. Introduction

The observation of very-high energy γ -rays (VHE; $E > 100$ GeV) from distant sources offers the unique possibility to probe the density of the meta-galactic radiation field at ultraviolet (UV) to infrared (IR) wavelengths, which is commonly labeled the extragalactic background light (EBL; typically 0.1-100 μm). The VHE γ -rays interact with the low energy EBL photons via the pair production process ($\gamma_{\text{VHE}}\gamma_{\text{EBL}} \rightarrow e^+e^-$) and the flux is attenuated [1, 2]. This attenuation can leave distinct signatures in the measured VHE spectra. With assumptions about the source physics and the spectrum emitted at the source location (intrinsic spectrum), constraints on the density of the EBL can be derived [e.g. 3, 4].

The current generation of VHE instruments (H.E.S.S., MAGIC, VERITAS) significantly increased the number of known extragalactic VHE sources from 4 in the year 2003 to more than 25 today. These discoveries, combined with the advanced spectral resolution of these instruments and the wide energy range they cover, led to new strong constraints on the EBL density, in particular at optical to near-IR (NIR) wavelengths [5, 6, 7]. Since these limits depend on assumptions about the source physics, the strong constraints also sparked intense discussions on the validity of the assumptions and possible caveats [e.g. 8, 9, 10, 11, 12, 13]. This discussion has not yet converged and there are interesting arguments for both sides.

Current generation systems have recently been upgraded (MAGIC-II) or the upgrades are under construction (H.E.S.S. II). These upgrades are mainly aimed to improve the overall sensitivity by a factor two to three and extend the energy range toward the lower energy regime of 20 to 100 GeV. This will lead to some improvements, but a quantitative difference or a breakthrough compared to the performance of the existing facilities will only be achieved with an order of magnitude improvement in sensitivity. The Next Generation Cherenkov Telescope Systems (NGCTS) are in the advanced planning phase aiming to achieve this order of magnitude improvement: the Cherenkov Telescope Array (CTA¹) [14] and the Advanced Gamma-ray Imaging System (AGIS²) [15]. Whereas CTA envisions to improve the sensitivity over a wide energy range from the few tens of GeV to the multi TeV regime, AGIS mainly concentrates on energies above 100 GeV, an extended field of view and an improvement of the angular resolution.

The potential of these upcoming experiments to probe the EBL is the topic of

¹<http://www.cta-observatory.org/>

²<http://www.agis-observatory.org/>

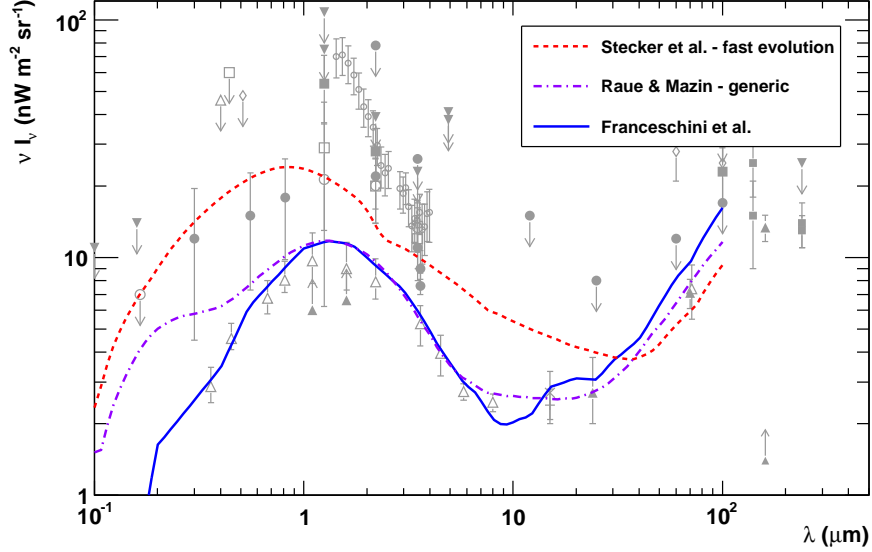


Figure 1: Present day ($z = 0$) EBL density of the EBL models/shapes utilized in this study (Stecker et. al. [16]; Raue & Mazin: [17]; Franceschini et al. [18]). Grey markers show measurements and limits on the EBL density (from [6]).

this article. While an order of magnitude improvement in sensitivity for an astronomical instrument will always lead to new and unexpected results, this article will - as a first step - focus on known results and their extrapolation according to the sensitivities of the next generation instruments. Emphasis will be on new techniques enabled by the performance features (extended sensitivity and energy range) of the upcoming instruments.

For the calculations in the paper a standard Λ CDM cosmology with $h = \Omega_\Lambda = 0.7$ and $\Omega_M = 0.3$ is adopted.

2. Basic assumptions and simulation details

EBL models and attenuation. The precise level of the EBL density is not well known. Solid lower limits from integrated deep galaxies counts at optical and infrared wavelengths do exist [e.g. 19, 20, 21, 22], but direct measurements are hampered by dominant foregrounds [23]. Over a large wavelength region in the infrared the best upper limits on the EBL density are derived from VHE observations of distant sources [e.g. 5, 6, 7]. To account for the uncertainty in the EBL density two different approaches are followed here: (i) To illustrate the effect of

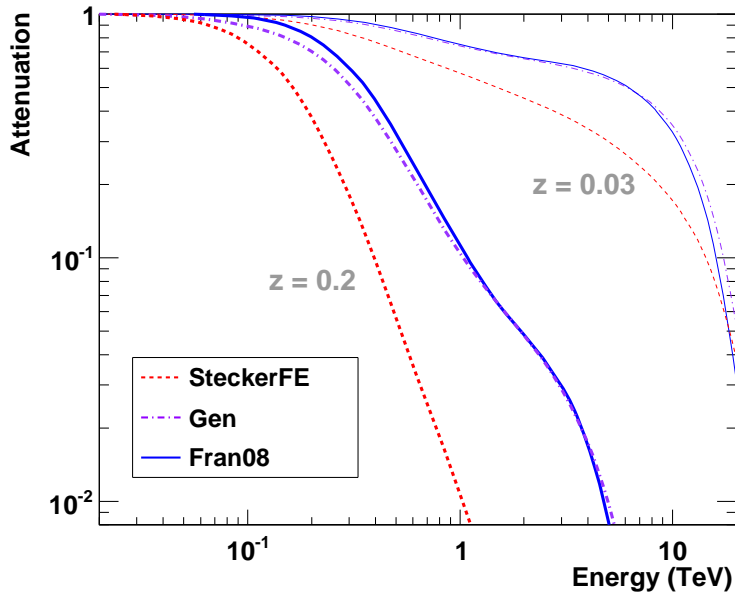


Figure 2: Attenuation for VHE γ -rays for the EBL models utilized in this study for sources at redshift $z = 0.03$ (thin lines) and $z = 0.2$ (thick lines).

the different EBL densities two extreme EBL models are used: for the low EBL density case the model from [18] (Fran08 in the following) is adopted, for the high model the fast evolution case from [16] (SteckerFE in the following) is used. It should be noted that the later model is already disfavored by several VHE observations. (ii) Detailed studies of the effect of different EBL densities are carried out by scaling the EBL density presented in [17] (Gen in the following) and Fran08. The present day EBL densities ($z = 0$) for the EBL models utilized in this work are displayed in Fig. 1

Fig. 2 displays the resulting attenuation for VHE γ -ray sources at 2 different redshifts ($z = 0.03$ and 0.2) for the models utilized. Several features can be identified:

- At low energies (< 80 GeV) the spectrum is practically not attenuated. Since this energy range will be sampled by the NGCTSs with high precision, it will be possible to measure the unabsorbed spectrum.
- At energies between 80 GeV and 2 TeV the attenuation is increasing due to the EBL photons in the optical to near-infrared range peak of the EBL density.

- At energies between 2 to 10 TeV a flattening of the attenuation is expected, due to the $\sim \lambda^{-1}$ behavior of the EBL density in the near to mid-infrared, resulting in a constant attenuation. Such a modulation of the EBL attenuation has been considered as a possible key signature for EBL attenuation [e.g. 24, 25]. Unfortunately, the intrinsic weakness of the sources combined with the sensitivity of the instruments make it very difficult to probe such a feature with previous or current generation experiments. For the SteckerFE model the EBL density in this wavelength range is flatter, resulting in a smoother attenuation from 100 GeV to 10 TeV, suppressing such a feature.
- At energies around 10 TeV the turnover in the EBL density towards the far-infrared peak of the EBL results in a strong attenuation, effectively resulting in a cut-off in the measured spectra.

The strength and the position of these features vary with the distance of the VHE sources, the assumed EBL model, and the overall EBL density.

EBL limits from VHE observations. So far, VHE sources used to derive limits on the EBL density belong to a single source class, active galactic nuclei (AGNs), and the majority of them to the Blazar sub-class, which are AGNs with strong jet activity and the jets are closely aligned to the line of sight of the observer. Up to now, mainly two different methods - and thereby assumptions about the source intrinsic spectrum - have been utilized to derive limits on the EBL density:

- *Spectral concavity.* It is assumed that the overall intrinsic source spectrum at high energies will follow a concave shape, or at least will not show an exponential rise towards the highest energies. These assumptions are well motivated by the common leptonic modeling of the sources under investigation (blazars), although different (maybe more exotic models) can possibly reproduce such a feature [e.g. 8]. Limits on the EBL density are derived by excluding EBL densities that would lead to such features in the observed sources. This method naturally probes the EBL at wavelengths from the mid to the far-infrared.
- *Maximum spectral hardness.* To probe the EBL in the optical to near-infrared, it is assumed that the intrinsic source spectrum cannot exceed a certain absolute hardness. While somewhat similar in spirit to the first method the underlying assumptions are stronger, since in the energy range of interest (100 GeV to several TeV) the spectral shape of the intrinsic spectrum is more uncertain. While most of the basic models used to describe the

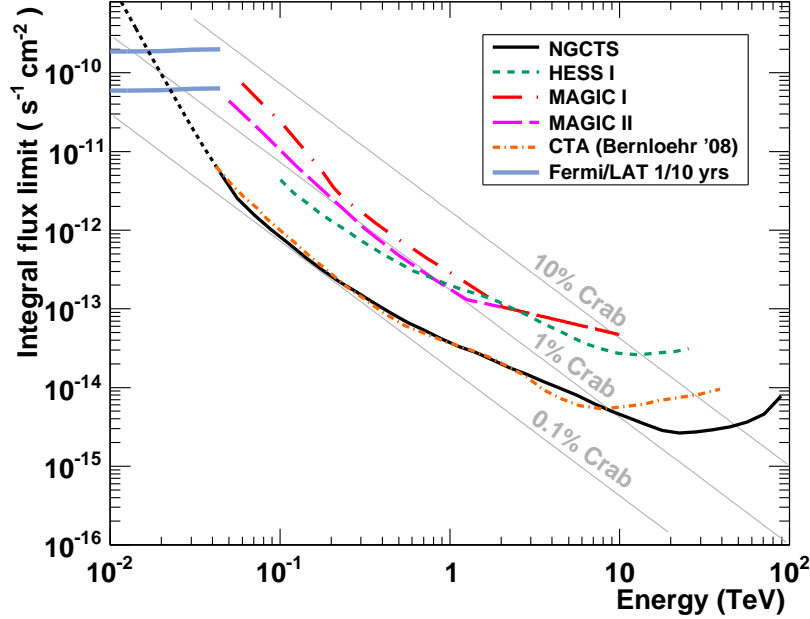


Figure 3: Integral flux sensitivity (5σ in 50h) of the NGCTS used in this study in comparison to the sensitivity of existing observatories (H.E.S.S.: [26]; MAGIC: [27]; *Fermi*: http://www-glast.slac.stanford.edu/software/IS/glast_lat_Performance.htm).

source spectra indeed imply that the VHE spectrum does not exceed a certain hardness, the absolute value is less certain³ and possible source intrinsic effect (e.g. internal absorption [11]) could complicated the situation.

In this paper two different methods to derive limits on the EBL density will be explored: (i) utilizing the unabsorbed part of the VHE spectrum and (ii) searching for attenuation modulation signatures. While not completely new, it will be shown that with the NGCTS's extended energy range paired with its vastly improved sensitivity it will be possible to utilize these methods effectively for the first time. Method (i) holds the potential to derive limits on the EBL density with a minimal set of assumptions, while method (ii) enables to not only derive upper limits on the EBL density but to probe the absolute level.

Effective area, background rate and sensitivity. To simulate the spectra, which will be detected by the NGCTS, assumptions about the sensitivity of the instru-

³e.g. $\Gamma = 1.5 - 0.6$ for $dN/dE \sim E^{-\Gamma}$ and simple leptonic models.

ment have to be made. As baseline sensitivity, the sensitivity of the "4 large + 85" CTA array presented in [26] is taken and the sensitivity is derived assuming an effective detector area (effective area) and a background rate. For the effective area the post cut MAGIC effective area at 20 deg zenith angle ([28]) scaled up by a factor 20 is adopted to reach an effective area exceeding 10^6m^2 at energies above a few hundred GeV. In addition, the MAGIC effective area is shifted by a factor of 2 to lower energies to reflect the improved sensitivity at low energies.⁴ The resulting effective area A_{NGCTS} versus energy E in the energy range 20 GeV to 20 TeV is well described by the function

$$A_{NGCTS} = 2.5 \cdot 10^{16}\text{m}^2(E/1\text{ TeV})^6(1 + (E/(1\text{ TeV} \cdot 0.02))^{0.9})^{-6/0.9} \quad (1)$$

The differential background rate after event selection cuts is approximated by a broken power law function with photon index 3.6 below and 2.7 above the break energy of 300 GeV, similar to what is seen in current generation instruments. The absolute level of the background flux rate is chosen so that the resulting sensitivity matches the sensitivity of the CTA "4 large + 85" array from [26]. The integral sensitivity adopted in this study for the NGCTS in comparison to current generation and future HE/VHE instruments is displayed in Fig. 3. In the overlap region it follows very well the CTA sensitivity for the "4 large + 85" array from [26] up to 10 TeV. Compared to current instruments (H.E.S.S., MAGIC, VERITAS) the sensitivity in the core energy range between 100 GeV and 10 TeV is improved by about one order of magnitude. In addition, the energy range is extended toward lower and higher energies. With the chosen parameters for the effective area and the background rate at low energies significant sensitivity is reached down to energies below 20 GeV, which enables a large overlap region in energy with the Large Area Telescope (LAT) onboard *Fermi* satellite. For this energy region, where there is no overlap with the published CTA sensitivity (<40 GeV), there is of course a certain degree of freedom in the choice of parameters and therefore the sensitivity is not very well constrained. In this study only energies between 40 GeV and 10 TeV will be used.

Spectrum simulation method. To calculate the simulated spectrum the number of γ -photon events N_S (signal) and background events N_{BG} per energy bin need to be

⁴The energy threshold approximately scales linearly with $1/\text{Area}$ of the mirror area of the single telescope. For a CTA type NGCTS instruments the largest telescopes are expected to have mirror diameter in the order of 24 m which gives a factor two larger area compared to 17m for the MAGIC mirror.

determined: the NGCTS effective area folded with the assumed intrinsic source flux is integrated over the energy bin; the same is done for the background events integrating over the background rate in the bin. Both numbers are multiplied with the effective observation time. Different functions are utilized to describe the intrinsic flux and they will be discussed further in the section where they first appear. The attenuation of the source flux due to the EBL is calculated following the recipe given in [6, 13]: the attenuation is directly folded into the intrinsic spectrum and then the attenuated intrinsic flux function folded with the effective area is integrated over the energy bin. The number of signal events is randomly varied assuming a Poisson distribution. It is assumed that the background is well determined (e.g. via background measurements in a large sky area compared to the signal region). The error on the number of photons N_σ in a bin is derived utilizing equation 17 from [29] assuming 5 background regions (i.e. an alpha factor of 0.2). The signal in an energy bin is considered significant when all of the following criteria are met: (1) the signal significance exceeds 3 standard deviations, (2) there are at least 10 excess events in the bin, (3) the number of excess events in the bin exceeds 3% of the number of background events. This last condition takes into account a systematic error in the determination of the number of background events. These are rather conservative assumptions, since e.g. in current publications on VHE γ -astronomy often energy bins with significances down to 1.5σ or less are included in the analysis.

IACT experiments have a limited energy resolution which, for current generation instruments, is in the order of $<15\%$ for energies above 100 GeV [e.g. 30] and $<40\%$ down to 70 GeV [28]. For MAGIC-II an energy resolution of $<25\%$ for energies down to ~ 50 GeV is achievable [see Fig. 3 of 31]. Due to the, on average, higher number of telescopes participating in each event and the increased mirror size of the large telescopes the energy resolution for an NGCTS is expected to improve further. Such an energy resolution paired with an energy spectrum unfolding method [e.g. 32] will enable to robustly reconstruct smooth spectral shapes (e.g. power law or log parabola) even down to low energies. The reconstruction of an EBL attenuation structure at mid-energies is possibly more affected by the limited energy resolution and this will be further discussed at the end of Sect. 4.

Simulation example. Fig. 4 displays simulated spectra for two sources and two assumed EBL densities for an observation time of 20 h. The intrinsic spectrum is assumed to follow a simple power law ($\Phi(E) = \Phi_0 \times (E/1 \text{ TeV})^{-\Gamma}$), with the parameters adopted so that the EBL attenuated simulated spectrum matches the measured one. Shown are results for 1ES 1101-232 ($z = 0.186$), a hard spectrum

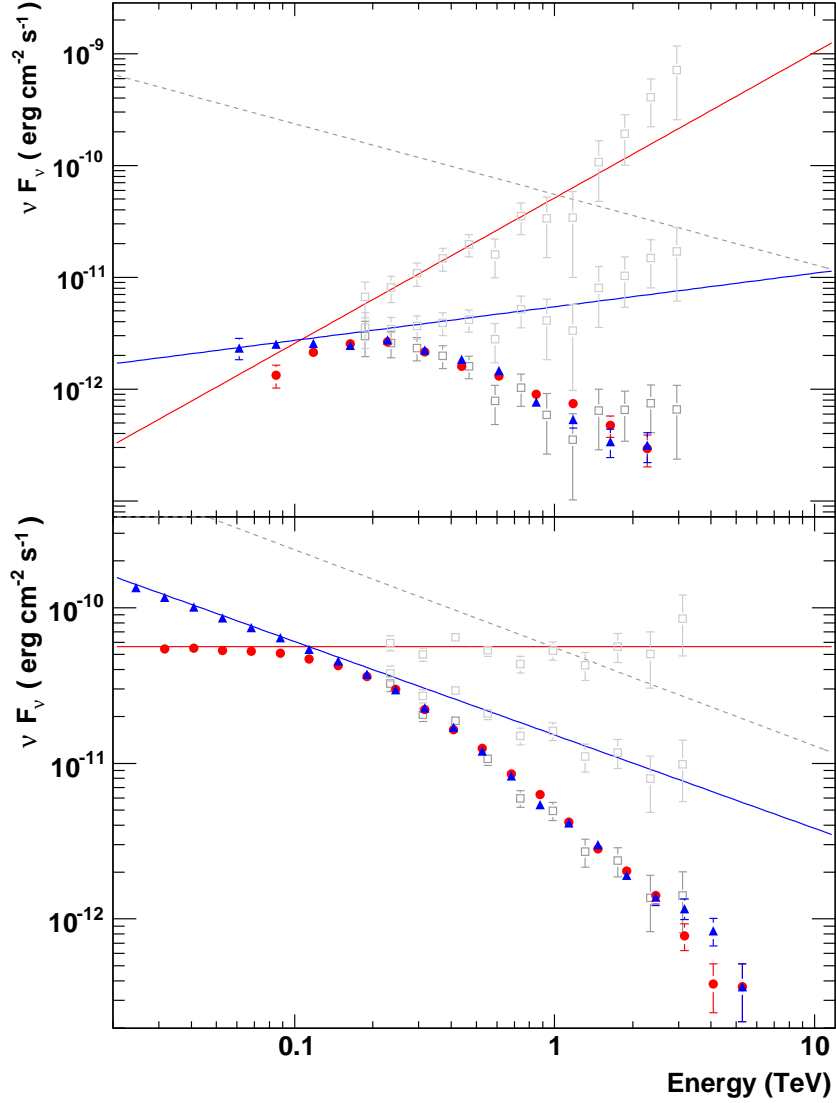


Figure 4: Simulated VHE spectra for two sources and two EBL models (blue: Fran08; red: SteckerFE). *Upper panel*: 1ES 1101-232. *Lower panel*: PKS 2155-304. Grey markers show the measured spectra and the measured spectra de-absorbed for EBL attenuation. Red and blue lines are the assumed intrinsic spectra emitted at the source for two different levels of the EBL density, matching the measured de-absorbed spectra. Red and blue markers show the expected spectrum as measured for a next generation VHE instruments simulated in this work. The dashed line gives the flux of the Crab Nebula. Spectral points below 40 GeV are only shown for illustrative purpose and are not used in the analysis.

($\Gamma_{VHE} \sim 3$) distant source, whose discovery at VHE energies enabled to derive strong limits on the EBL density in the optical to near-infrared [5], and PKS 2155-304, which is a fairly strong VHE source (about 20% Crab in the quiescent state) with a softer spectrum ($\Gamma_{VHE} \sim 3.3$) located at an intermediate redshift of $z = 0.116$. In the case of 1ES 1101-232 the hard measured spectrum in combination with the larger distance leads to a very hard intrinsic spectrum (i.e. harder than anticipated by simple leptonic and hadronic models), even for the low EBL model. Such a hard intrinsic spectrum coupled with the relative weakness of the source ($\sim 2\%$ Crab) leads to a simulated spectrum which does not largely increase the energy range covered compared to the H.E.S.S. measurement of 1ES 1101-232: neither at low energies (due to the hard spectrum) nor at high energies (the strong EBL attenuation suppresses the signal below the NGCTS sensitivity). Even for the case of the two very different assumed EBL models, no strong difference in the simulated spectra is apparent, which could be used to differentiate between the models. This is different in the case of PKS 2155-304, where, for the different EBL models, very different spectra are expected to be measured at lower energies. The behavior at low energies will be discussed further in the next section.

3. Utilizing the unabsorbed part of the spectrum

One of the main features of a NGCTS will be a high sensitivity in the energy range between 20 and 100 GeV, an energy range which holds the possibility to directly sample parts of the energy spectrum of a source, which are not affected by the EBL attenuation. In this section it will be explored how this energy range can be utilized to derive limits on the EBL density, and what are possible problems and caveats.

Simulation & analysis chain. The following simulation and analysis chain is utilized:

1. Calculate EBL attenuation for a specific EBL density and source distance.
2. De-attenuate a measured spectrum and fit with power law ($dN/dE = \Phi_0 \cdot E^{-\Gamma}$). The fit results serve as input flux function for the simulated spectrum.
3. Simulate spectrum as measured by an NGCTS with calculated input flux function.
4. Fit simulated spectrum in a low energy regime (intrinsic spectrum) and high energy regime (absorbed spectrum). Again, a simple power law function is used in each energy regime.

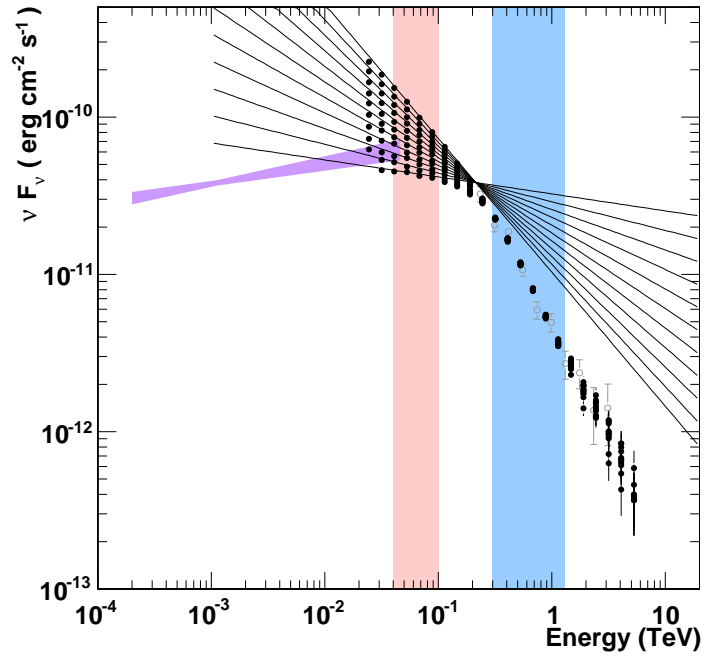


Figure 5: Example of simulated spectra for different EBL densities. The base spectrum assumed is the quiescent state spectrum of PKS 2155-304 ($z = 0.116$), EBL model is from Fran08. Shown are: the measured spectrum (grey markers), the simulated spectra for different level of the EBL density (black markers) and the corresponding assumed intrinsic spectra (black lines), the source spectrum in the GeV energy range as measured by Fermi [33] (purple butterfly), and the energy ranges which are used to determine the slope of the simulated spectrum at low (blue) and high (red) energies. Spectral points below 40 GeV are only shown for illustrative purpose and are not used in the analysis.

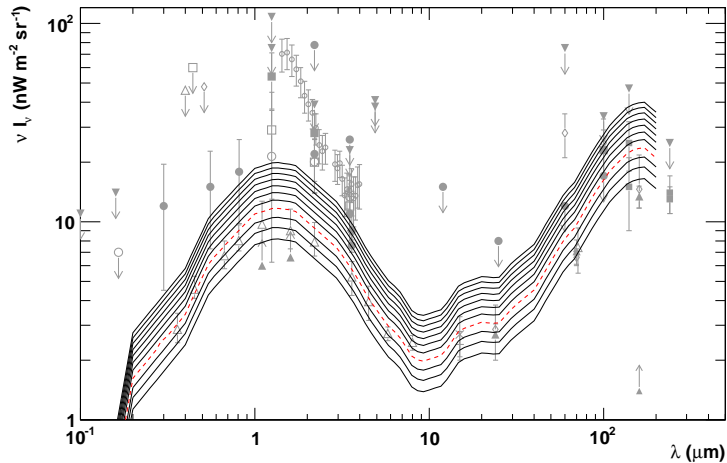


Figure 6: EBL density ($z = 0$) for the Fran08 EBL model scaled with a factor 0.7 to 1.7 in steps of 0.1. The red dashed curve is the unscaled EBL model.

5. 200 spectra are simulated and mean values are used.

An example for this procedure is shown in Fig. 5 for the quiescence spectrum of PKS 2155-304 ($z = 0.116$). An observation time of 20 h has been assumed, which could easily be extended given that this is a steady flux state. As EBL model the Fran08 model is used, scaled in steps of 0.1 from 0.7 to 1.7 (Fig. 6).

Fit-range & source intrinsic break. The resulting EBL attenuations for the scaled models are shown in Fig. 7 upper left panel. The energy ranges used to fit the power laws are marked by colored boxes. In the high energy range the attenuation follows approximately a power law and since the input spectrum is also a power law, the resulting attenuated spectrum will follow a power law as well. In the low energy range no significant absorption is present. As recent *Fermi*/LAT observations show, a spectral break is observed between the GeV and the TeV energy range [34]. For many sources this break can be attributed to a break expected from EBL attenuation. For these sources an NGCTS would be able to sample the intrinsic spectrum down to very low energies. In other cases, e.g. PKS 2155-304, the break between GeV and TeV range is stronger than expected from EBL attenuation, therefore an additional, source intrinsic break is expected somewhere between the two energy bands. Currently, the statistics for this energy range for the sources considered here is not yet sufficient to correctly model the break. Therefore, for the analysis in this paper the lower edge of the low energy

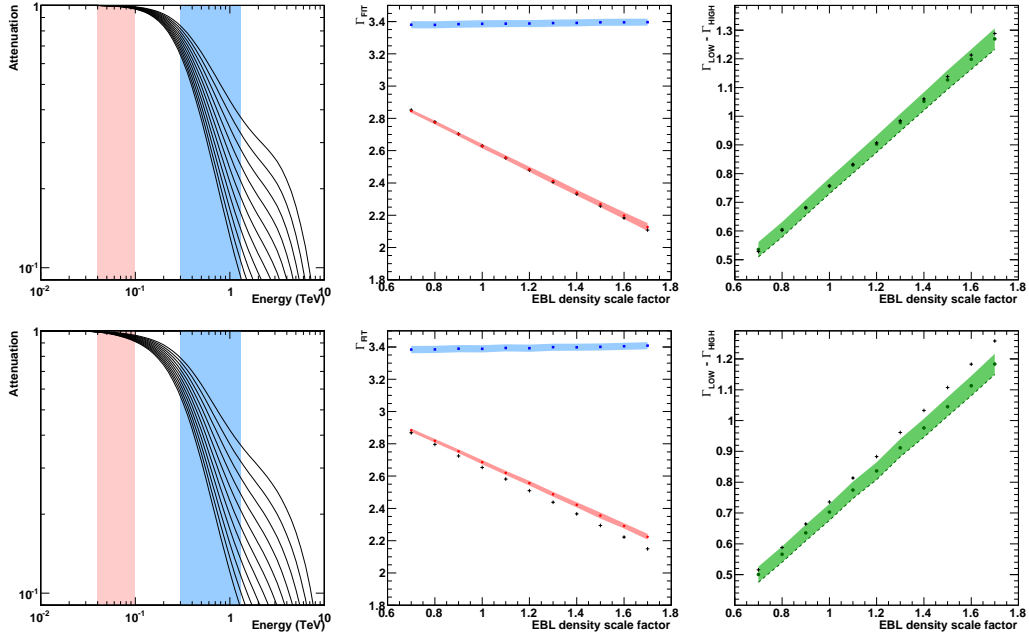


Figure 7: Results from the power law fit to the simulated spectrum in the low and high energy band using the PKS 2155-304 quiescence spectrum with the Fran08 (upper row) and Gen (lower row) EBL model. *Left:* Attenuation of the VHE γ -ray flux resulting from the scaled EBL models. The colored boxes in the background mark the fit range for the power law at low (red) and high (blue) energies. *Middle:* Spectral index Γ from the fit of a power law to the low (red) and high (blue) energy range versus the scaling factor of the EBL model. The color shaded bands denote the error on the spectral index from the fit (RMS of the spectral index distribution). Black crosses mark the intrinsic spectral index that has been utilized. *Right:* Spectral break between low and high energies (error bands from error propagation). For discussion see main text.

fit range is chosen to start above the *Fermi*/LAT energy band (defined as the 5th highest photon in energy reported in [33], e.g. ~ 40 GeV for PKS 2155-304). Future observations with *Fermi*/LAT, MAGIC-II, and H.E.S.S. II will provide further information on this issue.

EBL attenuation spectral break. Fig. 7 upper middle panel shows the spectral index resulting from the power law fit for the two energy bands for the different scalings of the EBL model. The markers show the mean spectral index of the fits, with the error given as the RMS of the mean spectral index distribution (shaded bands). As alternative error definition the mean error on the spectral index from the fit could be used which gives similar results. The black crosses mark the spectral index utilized for the input source spectrum. It can be seen that the fit in the low energy band reproduces very well the assumed intrinsic spectral indices.⁵ For the highest scaled EBL densities the effect of attenuation becomes relevant in the low energy band and the spectral index from the fit is steeper (larger) than the one from the input spectrum. This effect will be discussed in more detail below. The right panel of the figures displays the strength of the spectral break between the two power laws $\Gamma_{LOW} - \Gamma_{HIGH}$, with the error bands calculated via error propagation. An EBL density scale factor of 0.1 corresponds to one to two standard deviations difference in the strength of the break.⁶ Note that a scaling of 0.1 corresponds to an EBL density of ~ 1 nW m⁻²sr⁻¹ at $2 \mu\text{m}$ which is of the same order as the error on the lower limits from integrated source counts at this wavelength. The detection of a break with certain strength can be converted into an upper limit of the EBL density (thick dashed line). In principal, a single well measured spectrum is sufficient to derive such limits. Since EBL attenuation is a global, redshift dependent phenomenon, in general, a combined fit to all available VHE data should be used to derive limits on the EBL density [see e.g. 6]. This is discussed in more details in Sect. 5.

EBL attenuation at low energies. The same analysis has been performed utilizing the Gen EBL model and the results are displayed in Fig. 7 lower row. The Gen EBL density in the ultraviolet to optical is higher than in the Fran08 model (Fig. 1), therefore resulting in a non negligible attenuation in the low energy band

⁵The correlation between the EBL density and the spectral index in the low energy band is a result of the methodology i.e. for each EBL density a corresponding intrinsic spectrum is constructed.

⁶I.e. if the Fran08 EBL model is correct and the intrinsic spectrum follows a power law in the energy range considered a 1.3 scaling of the model could be excluded with 3 standard deviations.

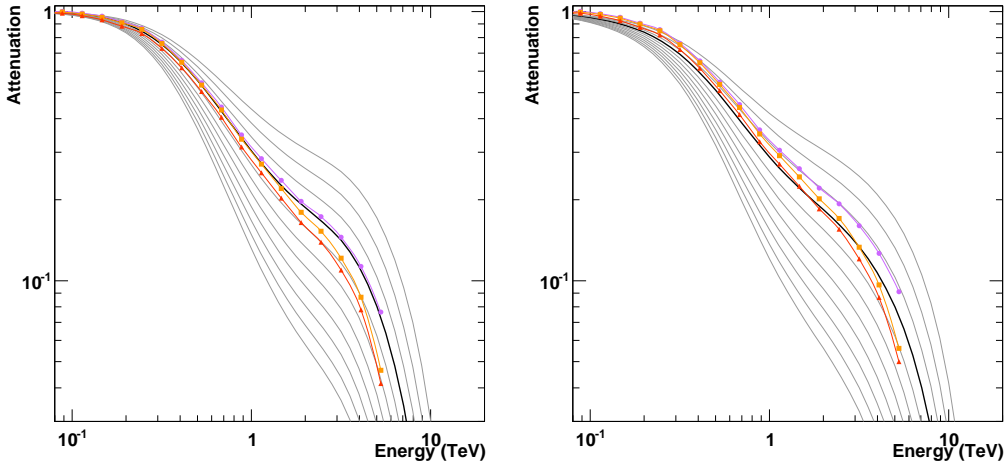


Figure 8: Energy dependent upper limits on the attenuation for the Fran08 (left) and the Gen (right) EBL models derived utilizing the PKS 2155-304 quiescence spectrum. Shown are the limits taking into account the 1σ error on the flux points (orange filled squares), with the addition of the 1σ error on the spectral index of the low energy power law (red filled triangles), and no errors (purple filled circles). The black line shows the attenuation for the EBL model utilized, grey lines show the attenuation for the EBL model scaled in steps of 0.1.

(Fig. 7 lower left panel). Consequently, the power law fit in the low energy band results in a too soft spectrum compared to the input source spectrum (Fig. 7 lower middle panel). This mis-reconstruction, if taken at face value, would lead to an overestimated upper limit on the EBL density (Fig. 7 lower right panel). To be able to utilize the low energy part of the spectrum as proxy for the intrinsic spectrum it is therefore crucial to carefully examine the spectral shape in the energy range for signs of curvature. A conservative approach would be to correct the flux points in the fit energy range for the attenuation from a maximum EBL before performing the fit. On the other hand, if a high statistic VHE spectrum from a distant source does not show any indication of curvature in this energy regime, tight limits on the EBL density in the ultraviolet to optical EBL can be derived.

Energy dependent attenuation limits. The power law fit to the low energy region, if taken as proxy for the intrinsic spectrum, can also be used to derive energy dependent upper limits on the attenuation. Such limits can be extremely useful: the EBL attenuation is an energy dependent process, where certain wavelength regions of the EBL spectrum are connected to certain VHE energy ranges. Features in the EBL density, as e.g. expected from the first stars [see e.g. 35], could

therefore also produce features in the attenuation. The resulting energy dependent EBL attenuation limits from such an analysis for the Fran08 and the Gen EBL model utilizing the PKS 2155-304 quiescent spectrum are shown in Fig. 8⁷. As can be seen from the figure, the dominant source of errors in such an analysis are the uncertainties on the spectral index from the power law fit in the low energy range, since the statistical errors on individual flux points are comparably small. Again, the rejection power is in the order of $1-2\sigma$ per 0.1 scaling of the EBL density at energies > 1 TeV, when utilizing a simple and ad-hoc error definition. In the case of the Gen EBL model again the effect of the attenuation "spill over" in the low energy fitting band is visible: due to the EBL attenuation the power law fit is too soft, resulting in an underestimated EBL attenuation and too strong limits.

Flaring states. Up to here only the quiescent flux state of sources has been considered, since its observation is guaranteed. AGNs do also show extreme flaring behavior with high fluxes, unfortunately usually only for short periods of time. Here, the VHE spectrum recorded during the extreme flux outburst of PKS 2155-304 in 2006 [36] is investigated. The spectrum is an averaged spectrum of 1.5 h of observations, in which the source showed several strong flares with time-scales down to a few minutes. While no strong spectral variations in the VHE spectrum have been observed during this flare, for the analysis only short observations of 6 min length have been considered, demonstrating the power of the NGCTS to derive high quality spectra even on such short time-scales. In addition, the EBL attenuation is a "stationary" effect in the spectrum, therefore a temporally fine resolved flaring state might enable to distinguish between intrinsic and EBL effects. The resolution of the EBL density achieved for such a 6 min observation of the source in a flaring state is comparable with the one achieved for 20 h of quiescence observations (Fig. 9 top row).

Nearby sources. Strong flux outbursts in the VHE regime have also been observed in the two nearby sources Mkn 421 and Mkn 501. While the smaller distances result in less EBL attenuation and therefore a weaker signature, the overall higher flux levels of these two sources enable to derive spectra with high event statistics. Here, the time-averaged VHE spectrum of Mkn 501 during the 1997 high state is investigated, assuming an observation time of 20 h. As can be seen from Fig. 9 bottom row, while the overall strength of the break between the two power laws is

⁷For this investigation only a single simulated spectrum without applying the statistical dicing of the event numbers is used.

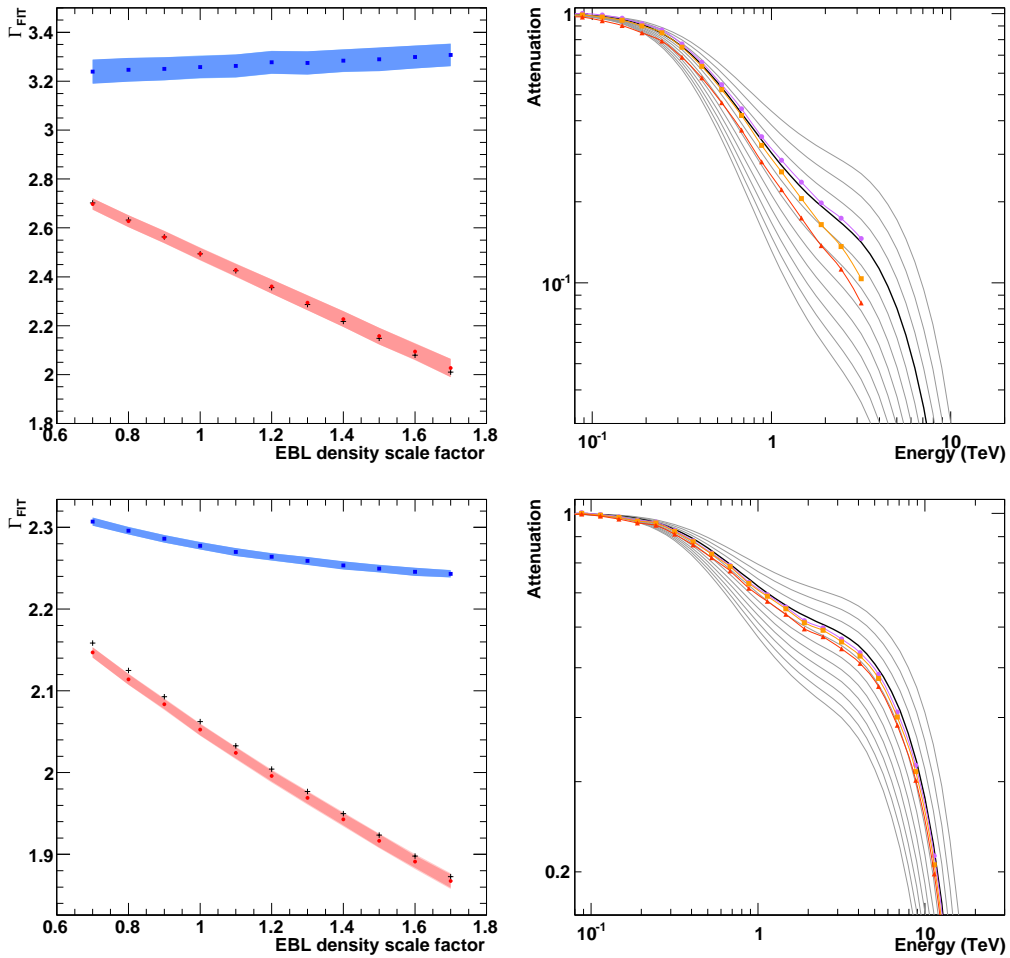


Figure 9: EBL limit results from power law fits to low and high energy bands of the VHE spectrum using scaled version of the Fran08 EBL model (see Fig. 7 and 8 for detailed description). *Upper row*: Results for the VHE spectrum from the flaring state of PKS 2155-304 in 2006 [36] (6 min observation time), *Lower row*: Results for the averaged high state spectrum of Mkn 501 [37] ($z = 0.034$; 20 h observation time).

much smaller than in the case of PKS 2155-304 (0.15–0.4 vs 0.5–1.2) comparable limits can be derived due to the superior statistics. In addition, the problem of attenuation in the low energy band is less severe. One caveat - at least for the case of Mkn 421 - is the fact that there are strong indications for an intrinsic (not EBL related) break between the GeV and TeV range at relatively high energies (around 100 GeV) [34], which would make it difficult to define a proper low energy region void of any curvature. A different method, discussing the possibilities of how such high quality spectra with a wide energy range produced by a nearby source can be used to test the EBL density, is discussed in the next section.

4. Attenuation modulation at mid-energies

The NGCTS will achieve an unprecedented sensitivity in the intermediate energy range, i.e., between 100 GeV and few TeV. For nearby sources, this energy range is most sensitive for the EBL density in the optical to infrared regime ($\sim 1\text{--}15\ \mu\text{m}$), which can, thus, be probed very efficiently with an NGCTS measurement of an AGN energy spectrum.

Smoothness of AGN spectra. The measured energy spectra of AGNs in the energy range between 100 GeV and few TeV follow usually a smooth shape. For most of the measured sources, a simple power law fit is sufficient to describe the available data well, whereas for sources in a flare state (like the flare of PKS 2155-304 in 2006) or with a generally high emission state (like Mkn 421), either a curved power law or a power law with a cut-off are successfully used. The curved power law (also known in the literature as the double-log parabola) is expected to describe the spectra well at energies close to the position of the Inverse-Compton peak. The power law with a cut-off instead is the expected behavior of a source which does not provide necessary conditions for acceleration of charged particles to sufficiently high energies. All scenarios do have one common feature: the measured spectra can be described by smooth functions, i.e., no features, wiggles or pile-ups are expected, especially after de-convolving the spectra for the effect of the EBL absorption. This property can, therefore, be used to distinguish between different overall EBL levels in the optical to infrared regime: whereas the "correct" EBL model and level will produce a smooth intrinsic AGN spectrum, an "incorrect" EBL level would result in a signature (in form of well defined wiggles) in the reconstructed intrinsic spectrum.

The strength of the method is that the EBL signatures in the reconstructed AGN spectra will not only be visible (measurable) in the case where the assumed

EBL level is higher than the real one, but also in case the assumed EBL level is lower than the real one. It is, therefore, the first indirect method to really measure the EBL density at $z=0$.

Simulation & analysis chain. The utilized methodology is sketched below:

1. Assume an intrinsic spectral shape and the flux level of a known strong extragalactic gamma-ray source.
2. Simulate NGCTS spectrum assuming the absorption due to the standard EBL, i.e., with the scaling factor of 1.
3. Reconstruct intrinsic spectrum of the source assuming a scaled EBL level. For a scaling, which is different enough from the standard EBL, the reconstructed AGN spectrum will show distinct wiggles.
4. To characterize the presence of the wiggles, a fit by a smooth source function (spectral shape) is performed. The chosen fit shape is the curved power law: $dN/dE = N_0 \times \left(E^{-\alpha+\beta \log(E/E_0)} \right)$
5. The resulting χ^2 of the fit is then used to judge if the change in the EBL level results in an improbable reconstructed intrinsic spectrum.
6. Repeat the simulation 1000 times for the given EBL scaling and compute the mean and the RMS of χ^2 values from the fits to the reconstructed intrinsic spectrum.

Simulation example. The steps 1–4 of the method are illustrated in Fig. 10 for the VHE spectrum of Mkn 501. The assumed spectral shape and the flux level of the intrinsic spectrum are adapted to the flux measured by HEGRA [37] during the outburst of the source in 1997: the original data are shown by grey open squares in the upper panel of the figure. The simulated NGCTS spectrum calculated using the 'correct EBL' (Gen EBL model; scale factor 1) is shown in red, whereas the assumed intrinsic spectrum of Mkn 501 is shown by the solid grey line and the reconstructed intrinsic spectrum is shown by the blue filled circles. The effect of the mis-reconstruction of the intrinsic spectrum is shown for the example of an EBL scaled by a factor of 1.3: the reconstructed intrinsic spectrum (green filled triangles) clearly shows wiggles in the fit range. The effect of the wiggles is more visible in the lower panel of the figure where the residuals to the best fit function are shown. The wiggles are quantified by a fit in the energy range between 100 GeV and 7 TeV, well before a possible pile-up in the spectrum arises. The choice of the fit range is made in order not to bias the result by the level of the EBL above

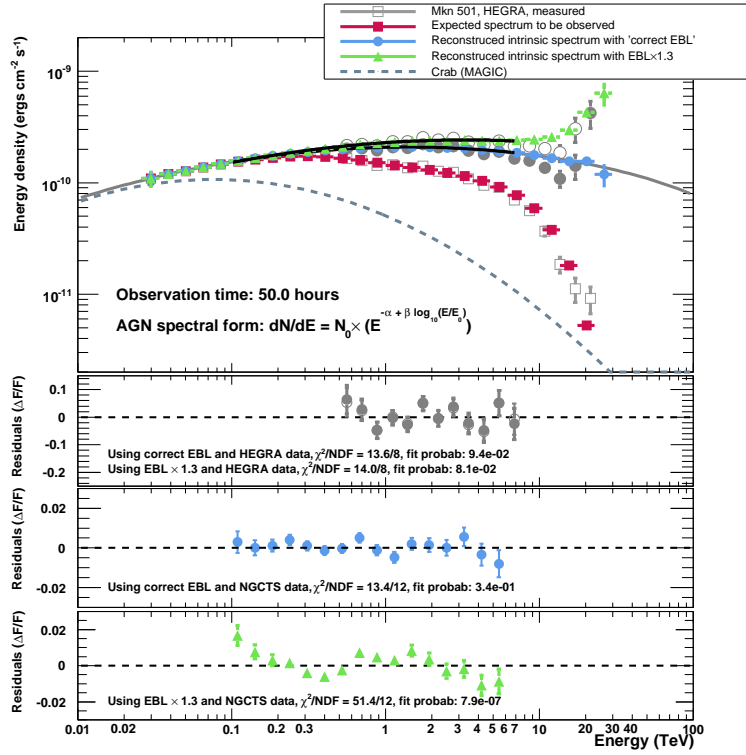


Figure 10: Search for signatures at mid-VHE in the Mkn 501 spectrum. *Top panel:* The Mkn 501 spectral energy distribution (SED) at very high energies. Shown are: measured spectrum by HEGRA (grey open squares), simulated NGCTS spectrum (red filled squares), assumed intrinsic spectrum of Mkn 501 (grey solid line), reconstructed intrinsic Mkn 501 spectrum (blue filled circles) and reconstructed intrinsic spectrum of Mkn 501 assuming an EBL scaling factor of 1.3 (green triangles). For comparison, the deabsorbed HEGRA Mkn 501 is shown for the same two EBL models (filled grey circles and open grey circles, respectively). The Crab Nebula spectrum (grey dashed line) is shown for comparison. *Middle upper panel:* Residuals of the fits to the de-absorbed HEGRA Mrk 501 spectrum for the case of the two different assumptions about the EBL density. The difference between the two curves (filled and open circles) is very small. The HEGRA sensitivity is not sufficient to decide between the two assumptions. *Middle lower panel:* Residuals between the best fit to the SED in case of NGCTS measurement and the spectral points from the intrinsic spectrum using the correct EBL density. *Bottom panel:* Residuals between the best fit to the SED for a NGCTS measurement and the spectral points from the intrinsic spectrum reconstructed using the scaled EBL model. A clear and significant signature (wiggles) in the residuals is visible, which is quantified by a low probability of the fit.

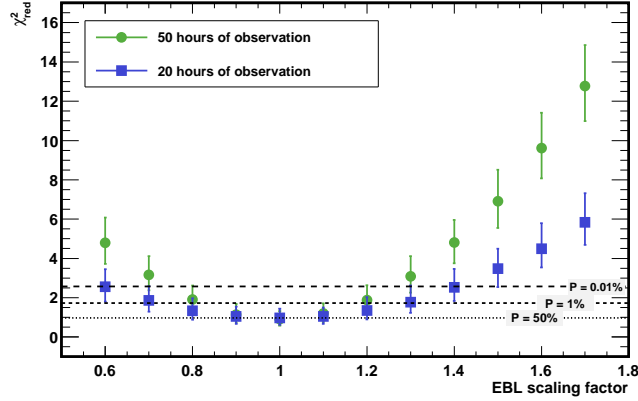


Figure 11: Quantitative results from the search for EBL signatures in the mid-VHE using the energy spectrum of Mkn 501. Shown are the reduced χ^2 values from the fits to the reconstructed spectra of Mkn 501 as a function of EBL scaling factor. Blue filled squares and green filled circles show the expected result for 20 and 50 hours of NGTCS observations, respectively. The black horizontal lines correspond to fit probabilities as labeled.

$10\mu\text{m}$, to which the VHE spectra are very sensitive due to a super exponential dependency of the attenuation with the wavelength in that range. Using the correct EBL level to reconstruct the intrinsic spectrum, the intrinsic spectrum is well described by a smooth function (Fig. 10, middle lower panel). Instead, when using a "wrong" scaled EBL density characteristic deviations (wiggles) from a smooth function are visible (Fig. 10, lower panel). The wiggles are quantified by a reduced χ^2 value of $51.4/12$, corresponding to a fit probability of $7.9 \cdot 10^{-7}$. The small fit probability for the assumed scaled EBL level implies (under used assumptions) significant presence of the unphysical wiggles and, therefore, an exclusion of that particular EBL realization. For comparison, HEGRA measured spectrum is also de-absorbed using the same two EBL models and the results are shown by grey filled and open circles in the upper panel. The residuals to the best fits are shown in the middle upper panel. The difference between the two curves (represented by grey filled and open circles) is not significant and is difficult to see. The similar reduced χ^2 values of $13.6/8$ and $14.0/8$ underline that the HEGRA measurement was not sensitive to the method.

Results of the analysis. This procedure is repeated 1000 times for every scaled EBL density in order to achieve a solid statistical mean and a 1σ (68%) coverage of the reduced χ^2 values. The results are shown in Fig. 11 for two different NGTCS exposures (20 and 50 hours) plotting the mean reduced χ^2 values in-

cluding 68% error bars versus the EBL scaling factor. As a result one can see a parabola-like curve with the minimum at EBL scaling factor of 1.0, which is via construction the correct EBL model. The expected mean reduced χ^2 values are shown by the blue filled squares and the green filled circles for the exposures of 20 hr and 50 hr, respectively. The corresponding fit probabilities of P=50%, 1% and 0.01% are shown by the dotted, short-dashed and long-dashed lines, respectively. An EBL scaling is considered to be excluded when the mean reduced χ^2 value including its 68% error exceeds the χ^2 value for P=0.01%. For the case constructed here this means that in case of 50 hours observation, the EBL scalings below 0.65 and above 1.35 are excluded. In the case of 20 hours observation, the EBL scalings above 1.50 are excluded.

Caveats of the method. The method presented above is not only sensitive in constraining the EBL density but it is also a first attempt to resolve the actual EBL level. Still, the method has several caveats: (i) There is a possibility that the intrinsic VHE spectrum is not smooth for some AGNs. For example, several emission regions or several generations of charged emitting particles (e.g., electrons) may produce spectral features which would mimic the signature from a wrong EBL model. Though neither the AGNs observed at low energies with Fermi/LAT, nor the extragalactic VHE γ -ray sources observed so far with IACTs have shown structured spectra, such wiggles can be interpreted as the result of a wrong EBL model only if found to exist in several spectra of different sources consistently. (ii) The spectral signature shown in Fig. 10 can only be recognized well after a long exposure of a source being in a flare state. The data of the Mkn 501 flare from 1997 used for the study remains unique so far. This means that it cannot be expected that a study with such precision can be done on many sources with future NGCTS. Still, the indirect EBL measurement based on few strong flares will be of high importance. (iii) The limited energy resolution of IACTs ($\sim 10\%$) could affect the possibility of detecting such a signature. The overall shape of the attenuation effect is broad enough in energy to not strongly be affected by the smoothing of an energy resolution of $< 10\%$. For nearby sources, however, the wiggle structure produced by the wrongly assumed EBL model is only of order of a few per cent of the total flux level. An additional spread introduced by the spill-over effects due to events with mis-reconstructed energy may enhance or alter the wiggles. Therefore, an efficient and precise spectral unfolding technique will be key to overcome these problems for nearby sources. For more distant sources the attenuation signatures get quickly stronger. It will be, therefore, highly interesting to study a strong flaring state from a source at redshift $\gtrsim 0.1$ with the NGCTS.

5. Summary & Conclusions

In this paper the potential of a Next Generation Cherenkov Telescope System (NGCTS) to study the EBL through observations of VHE spectra from distant sources is explored. In the focus of the study lies the energy range between 40 GeV and 10 TeV, where a factor 10 improvement in sensitivity over current generation experiments is expected. Two different methods are investigated: (i) utilizing the unabsorbed part of the VHE spectrum in the energy range 40-100 GeV and (ii) searching for attenuation modulation signatures at energies between 100 GeV to 7 TeV. While some caveats, like e.g. the exact shape of the intrinsic spectra, do exist, overall the two methods show promising results, clearly go beyond what is possible with current generation instruments.

EBL attenuation is a global phenomenon that affects the spectra of all sources in the same way. It is therefore quite natural to expand the studies on the EBL by combining the results from different methods, sources or source flux states. This can e.g. be done by utilizing log-likelihood methods to combine the constraints from different sources and methods. In addition only the low and mid-VHEs have been investigated. At energies > 10 TeV further signatures from EBL attenuation ("cut-off") are expected, which have been used extensively in the past to derive limits on the EBL density in the FIR.

In this paper only data from a single instrument - a NGCTS - and minimal assumptions about intrinsic spectrum have been used to derive constraints on the EBL density. AGNs are observed all across the electromagnetic spectrum and the theory predicts connections between the observations at different energies. A wealth of multi-wavelength information is therefore accessible, which - in combination with a theoretical model - can be used to constrain the spectrum at VHE. A first model-dependent approach to determine the EBL level using a consistent SED modeling of detected blazars was discussed recently by [38]. While a detailed discussion of this topic is beyond the scope of this paper, as an example it should only be mentioned the power of combining the *Fermi* observations at MeV to GeV energies with observations from an NGCTS: such observations will cover over 9 decades (!) in energy with high precision.

The sources under study show strong flux variability in the VHE band. The high sensitivity of a NGCTS will enable to study the energy spectrum on very short time-scales in great detail. The time resolution will enable stronger constraints on the theoretical modeling of the source spectra since the experimental data will be available on shorter scales than the relevant changes in the emission regions. This will further help to disentangle source intrinsic effects and EBL

attenuation.

In this study only the VHE spectra of a few selected known sources have been investigated. The NGCTS will bring new discoveries. With the high sensitivity in the 20 to 100 GeV range it will be possible to detect fainter sources and sources at higher redshift. A (sufficiently) large sample of sources will serve a two-fold purpose: (1) help to improve the understanding of the intrinsic source physics and (2) enable statistical studies of the EBL effects, e.g. by investigating the EBL attenuation features versus redshift. This will also enable to not only probe the present day EBL but to study its evolution with redshift. How such a study can be performed with the help of an NGCTS will be the topic of a second paper.

Acknowledgments

MR and DM would like to thank M. Persic and M. Tluczykont for the careful reading of the manuscript and useful comments. MR and DM acknowledge fruitful discussion on CTA performance with J. Hinton and D. F. Torres. The authors would like to thank the referee for helpful comments and suggestions which improved the paper. DM acknowledges the support by a Marie Curie Intra European Fellowship within the 7th European Community Framework Programme.

Appendix A. References for VHE spectral data

Source name	Redshift	Reference
Mkn 501	0.034	[37]
PKS 2155-304	0.116	[39], [36]
1ES 1101-232	0.188	[5]

Table A.1: VHE spectra used in this publication.

References

- [1] A. I. Nikishov, Sov. Phys. JETP 14 (1962) 393.
- [2] R. J. Gould, G. P. Schröder, Opacity of the Universe to High-Energy Photons, Physical Review 155 (1967) 1408–1411. doi:10.1103/PhysRev.155.1408.

- [3] O. C. de Jager, F. W. Stecker, M. H. Salamon, Estimate of the Intergalactic Infrared Radiation Field from Gamma-Ray Observations of the Galaxy MARKARIAN:421, *Nature*369 (1994) 294–+. doi:10.1038/369294a0.
- [4] E. Dwek, J. Slavin, On the determination of the cosmic infrared background radiation from the high-energy spectrum of extragalactic gamma-ray sources, *ApJ*436 (1994) 696–704. doi:10.1086/174943.
- [5] F. Aharonian, A. G. Akhperjanian, A. R. Bazer-Bachi, et al., A low level of extragalactic background light as revealed by γ -rays from blazars, *Nature*440 (2006) 1018–1021. doi:10.1038/nature04680.
- [6] D. Mazin, M. Raue, New limits on the density of the extragalactic background light in the optical to the far infrared from the spectra of all known TeV blazars, *A&A*471 (2007) 439–452. arXiv:arXiv:astro-ph/0701694, doi:10.1051/0004-6361:20077158.
- [7] J. Albert, E. Aliu, H. Anderhub, L. A. Antonelli, P. Antoranz, et al., Very-High-Energy gamma rays from a Distant Quasar: How Transparent Is the Universe?, *Science* 320 (2008) 1752–. arXiv:0807.2822, doi:10.1126/science.1157087.
- [8] F. A. Aharonian, Proton-synchrotron radiation of large-scale jets in active galactic nuclei, *MNRAS*332 (2002) 215–230. doi:10.1046/j.1365-8711.2002.05292.x.
- [9] K. Katarzyński, G. Ghisellini, F. Tavecchio, J. Gracia, L. Maraschi, Hard TeV spectra of blazars and the constraints to the infrared intergalactic background, *MNRAS*368 (2006) L52–L56. arXiv:astro-ph/0603030, doi:10.1111/j.1745-3933.2006.00156.x.
- [10] A. Reimer, The Redshift Dependence of Gamma-Ray Absorption in the Environments of Strong-Line AGNs, *ApJ*665 (2007) 1023–1029. arXiv:arXiv:0705.1534, doi:10.1086/519766.
- [11] F. A. Aharonian, D. Khangulyan, L. Costamante, Formation of hard very high energy gamma-ray spectra of blazars due to internal photon-photon absorption, *MNRAS*387 (2008) 1206–1214. arXiv:0801.3198, doi:10.1111/j.1365-2966.2008.13315.x.

- [12] F. Krennrich, E. Dwek, A. Imran, Constraints on Energy Spectra of Blazars based on Recent EBL Limits from Galaxy Counts, *ApJ*689 (2008) L93–L96. arXiv:0810.2522, doi:10.1086/595960.
- [13] M. Raue, The Extragalactic Background Light: Lower Versus Upper Limits, *International Journal of Modern Physics D* 18 (2009) 1633–1637. arXiv:0904.2892, doi:10.1142/S0218271809015588.
- [14] G. Hermann, W. Hofmann, T. Schweizer, M. Teshima, f. t. CTA Consortium, Cherenkov Telescope Array: The next-generation ground-based gamma-ray observatory, *ArXiv e-prints* arXiv:0709.2048.
- [15] J. Buckley, K. Byrum, B. Dingus, A. Falcone, P. Kaaret, H. Krawczynski, M. Pohl, V. Vassiliev, D. A. Williams, The Status and future of ground-based TeV gamma-ray astronomy. A White Paper prepared for the Division of Astrophysics of the American Physical Society, *ArXiv e-prints* arXiv:0810.0444.
- [16] F. W. Stecker, M. A. Malkan, S. T. Scully, Intergalactic Photon Spectra from the Far-IR to the UV Lyman Limit for $0 < z < 6$ and the Optical Depth of the Universe to High-Energy Gamma Rays, *ApJ*648 (2006) 774–783. arXiv:astro-ph/0510449, doi:10.1086/506188.
- [17] M. Raue, D. Mazin, Optical depth for VHE γ -rays from distant sources from a generic EBL density, *International Journal of Modern Physics D* 17 (2008) 1515–1520. arXiv:0802.0129, doi:10.1142/S0218271808013091.
- [18] A. Franceschini, G. Rodighiero, M. Vaccari, Extragalactic optical-infrared background radiation, its time evolution and the cosmic photon-photon opacity, *A&A*487 (2008) 837–852. arXiv:0805.1841, doi:10.1051/0004-6361:200809691.
- [19] P. Madau, L. Pozzetti, Deep galaxy counts, extragalactic background light and the stellar baryon budget, *MNRAS*312 (2000) L9.
- [20] G. G. Fazio, M. L. N. Ashby, P. Barmby, J. L. Hora, J.-S. Huang, M. A. Pahre, Z. Wang, S. P. Willner, R. G. Arendt, S. H. Moseley, M. Brodwin, P. Eisenhardt, D. Stern, E. V. Tollestrup, E. L. Wright, Number Counts at $3 \mu\text{m} < \lambda < 10 \mu\text{m}$ from the Spitzer Space Telescope, *ApJS*154 (2004) 39–43. arXiv:astro-ph/0405595, doi:10.1086/422585.

- [21] D. T. Frayer, M. T. Huynh, R. Chary, M. Dickinson, D. Elbaz, D. Fadda, J. A. Surace, H. I. Teplitz, L. Yan, B. Mobasher, Spitzer 70 Micron Source Counts in GOODS-North, *ApJ*647 (2006) L9–L12. [arXiv:astro-ph/0606676](#), [doi:10.1086/507149](#).
- [22] H. Dole, G. Lagache, J.-L. Puget, K. I. Caputi, N. Fernández-Conde, E. Le Floch, C. Papovich, P. G. Pérez-González, G. H. Rieke, M. Blaylock, The cosmic infrared background resolved by Spitzer. Contributions of mid-infrared galaxies to the far-infrared background, *A&A*451 (2006) 417–429. [arXiv:astro-ph/0603208](#), [doi:10.1051/0004-6361:20054446](#).
- [23] M. G. Hauser, R. G. Arendt, T. Kelsall, E. Dwek, N. Odegard, et al., The COBE diffuse infrared background experiment search for the cosmic infrared background. i. limits and detections, *The Astrophysical Journal* 508 (1998) 25.
- [24] F. A. Aharonian, A. G. Akhperjanian, J. A. Barrio, et al., TeV gamma rays from the blazar h 1426+428 and the diffuse extragalactic background radiation, *A&A*384 (2002) L23.
- [25] L. Costamante, F. Aharonian, G. Ghisellini, D. Horns, The SED of the TeV BLLac 1ES 1426+428 after correction for the TeV-IR absorption, *New Astronomy Review* 47 (2003) 677–680. [arXiv:astro-ph/0301211](#), [doi:10.1016/S1387-6473\(03\)00121-0](#).
- [26] K. Bernlöhr, CTA simulations with CORSIKA/sim_telarray, in: F. A. Aharonian, W. Hofmann, & F. Rieger (Ed.), *American Institute of Physics Conference Series*, Vol. 1085 of *American Institute of Physics Conference Series*, 2008, pp. 874–877. [doi:10.1063/1.3076816](#).
- [27] T. Schweizer, Gamma-Ray Astronomy with MAGIC above 25 GeV, in: *International Cosmic Ray Conference*, International Cosmic Ray Conference, 2009.
- [28] J. Albert, E. Aliu, H. Anderhub, P. Antoranz, A. Armada, et al., VHE γ -Ray Observation of the Crab Nebula and its Pulsar with the MAGIC Telescope, *ApJ*674 (2008) 1037–1055. [arXiv:0705.3244](#), [doi:10.1086/525270](#).
- [29] T. P. Li, Y. Q. Ma, Analysis methods for results in gamma-ray astronomy, *The Astrophysical Journal* 272 (1983) 317.

- [30] F. Aharonian, A. G. Akhperjanian, A. R. Bazer-Bachi, et al., Observations of the Crab nebula with HESS, *A&A*457 (2006) 899–915. doi:10.1051/0004-6361:20065351.
- [31] P. Colin, D. Borla Tridon, E. Carmona, F. De Sabata, M. Gaug, S. Lombardi, P. Majumdar, A. Moralejo, V. Scalzotto, J. Sitarek, Performance of the MAGIC telescopes in stereoscopic mode, *ArXiv e-prints*arXiv:0907.0960.
- [32] J. Albert, E. Aliu, H. Anderhub, P. Antoranz, A. Armada, et al., Unfolding of differential energy spectra in the MAGIC experiment, *Nuclear Instruments and Methods in Physics Research A* 583 (2007) 494–506. arXiv:0707.2453, doi:10.1016/j.nima.2007.09.048.
- [33] A. A. Abdo, M. Ackermann, M. Ajello, W. B. Atwood, M. Axelsson, et al., Bright Active Galactic Nuclei Source List from the First Three Months of the Fermi Large Area Telescope All-Sky Survey, *ApJ*700 (2009) 597–622. arXiv:0902.1559, doi:10.1088/0004-637X/700/1/597.
- [34] A. A. Abdo, M. Ackermann, M. Ajello, W. B. Atwood, M. Axelsson, et al., Fermi Observations of TeV-Selected Active Galactic Nuclei, *ApJ*707 (2009) 1310–1333. arXiv:0910.4881, doi:10.1088/0004-637X/707/2/1310.
- [35] M. Raue, T. Kneiske, D. Mazin, First stars and the extragalactic background light: how recent γ -ray observations constrain the early universe, *A&A*498 (2009) 25–35. arXiv:0806.2574, doi:10.1051/0004-6361/200810396.
- [36] F. Aharonian, A. G. Akhperjanian, A. R. Bazer-Bachi, et al., An Exceptional Very High Energy Gamma-Ray Flare of PKS 2155-304, *ApJ*664 (2007) L71–L74. arXiv:arXiv:0706.0797, doi:10.1086/520635.
- [37] F. A. Aharonian, A. G. Akhperjanian, J. A. Barrio, et al., The time averaged TeV energy spectrum of MKN 501 of the extraordinary 1997 outburst as measured with the stereoscopic Cherenkov telescope system of HEGRA, *A&A*349 (1999) 11.
- [38] N. Mankuzhiyil, M. Persic, F. Tavecchio, High-frequency-peaked BL Lacertae objects as spectral candles to measure the Extragalactic Background

Light in the Fermi and air Cherenkov telescopes era, ApJLIn press.
arXiv:1004.2032.

- [39] F. Aharonian, A. G. Akhperjanian, A. R. Bazer-Bachi, et al., Multi-wavelength observations of PKS 2155-304 with HESS, A&A442 (2005) 895–907. doi:10.1051/0004-6361:20053353.